Research Square

Preprints are preliminary reports that have not undergone peer review.
They should not be considered conclusive, used to inform clinical practice,
or referenced by the media as validated information.

CSF synaptic proteins demonstrate region-wise associations with cerebral amyloid burden

Soha Alali
KU Leuven
Pourya Behmandpoor
Vrije Universiteit Brussel (VUB)
Pooya Ashtari
Ghent University
Koen Poesen
KU Leuven
Jolien Schaeverbeke
jolien.schaeverbeke@kuleuven.be

KU Leuven

Article

Keywords:

Posted Date: November 25th, 2026

DOI: https://doi.org/10.21203/rs.3.rs-11669418/v1

License: This work is licensed under a Creative Commons Attribution 4.0 International License.
Read Full License

Additional Declarations: No competing interests reported.

Abstract

Synaptic dysfunction and amyloid-β dysregulation arise early in the Alzheimer's disease continuum and appear closely intertwined during the disease trajectory. It is not fully understood how cerebrospinal fluid (CSF) synaptic proteins track with the spatial distribution of amyloid. This study included 35 individuals with mild cognitive impairment (MCI) from the Alzheimer's Disease Neuroimaging Initiative (ADNI) (80% amyloid-positive cases). Associations were explored between CSF synaptic proteins measured by SomaScan 7K and Florbetapir positron emission tomography (PET) across 17 amyloid-relevant brain regions using elastic net followed by linear regression adjusted for age, sex, *APOE* ε4, and education. Syntaxin-1A (STX-1A) and calsyntenin-3 (Clstn-3) showed the most extensive associations with amyloid burden, with the strongest associations in the dorsolateral prefrontal cortex for STX-1A (β = 0.52, $p_{\text{FDR-corrected}} = 3.24\times10^{-5}$) and the caudate nucleus for Clstn-3 (β=−0.49, $p_{\text{FDR-corrected}} = 0.017$). Most other synaptic proteins showed associations limited to specific regions, frequently including the lateral temporal and fusiform gyri. Mediation analysis indicated that associations were independent of gray matter volume loss. CSF synaptic proteins showed region-specific associations with cerebral amyloid burden, supporting their further evaluation as surrogate markers of amyloid pathology. These results underline that CSF synaptic proteins may follow different dynamics depending on the synaptic protein assessed.

INTRODUCTION

Amyloid-β (Aβ) deposition is a defining pathological feature of Alzheimer’s disease (AD), mainly affecting the cortical gray matter[1,2]. Amyloid positron emission tomography (PET) is currently the gold standard for *in vivo* detection and quantification of amyloid pathology[3,4]. Amyloid accumulation has been proposed to begin in temporobasal and frontomedial cortices[5], including early default mode network regions. These include the precuneus, posterior cingulate, and medial orbitofrontal cortex[6–8]. As the disease progresses, amyloid deposition progresses through broader associative neocortex and primary sensory-motor/medial temporal regions, ultimately reaching the striatum[5,9].

Before widespread amyloid deposition occurs, both i*n vivo* and *in vitro* evidence indicates that soluble Aβ oligomers act as early synaptotoxic species, preceding amyloid plaque formation and neuronal degeneration, directly interfering with synapse structure and function [10–13]. A key aspect is that Aβ plays a physiological role in regulating synaptic activity, as low concentrations of soluble Aβ contribute to normal synaptic function. This is consistent with a hormetic model in which tightly regulated baseline levels are required for synaptic health[12,14]. Disruption of this balance through excessive accumulation and pathological conformational change of Aβ marks the transition from physiology to disease[10,12,14]. Since synaptic dysfunction and Aβ dysregulation arise early in the AD continuum and appear closely intertwined during the disease trajectory, fluid biomarkers reflecting synaptic alterations may help illuminate cerebral amyloid pathology, particularly given the high cost and in some instances limited availability of amyloid PET[4].

Synaptic biomarker alterations appear to be stage- and protein-dependent across the AD continuum[15–19]. In cognitively unimpaired individuals at higher risk for AD, several synaptic proteins, including CSF Neurogranin (Ng), Growth-Associated Protein 43 (GAP-43), Synaptosomal-Associated Protein, 25 kDa (SNAP-25), and synaptotagmin-1 (Syt-1) increased with higher Aβ load. Interestingly, these changes were already detectable at early stages of Aβ deposition, measured by both CSF $A\beta_{42/40}$ and amyloid-PET Centiloid values[19]. Other evidence, however, points to non-monotonic trajectories: Vesicle-Associated Membrane Protein 2 (VAMP-2), SNAP-25, and Ng have been reported to be lower in the earliest asymptomatic AD stage than in controls, yet higher at later stages than during the asymptomatic stage[15]. Taken together, these findings suggest that certain synaptic proteins do not simply increase uniformly from the earliest stage but instead follow dynamic, stage-dependent trajectories during disease progression. Beyond the soluble N-ethylmaleimide-sensitive factor attachment protein receptor (SNARE) and postsynaptic markers, CSF proteomic studies have additionally reported increased Beta-synuclein, Gamma-synuclein, and several 14-3-3 isoforms in AD or amyloid-positive cohorts,[15,20–23] whereas neuronal pentraxins (NPTX), particularly NPTX2 and NPTXR, are generally reduced in AD and amyloid-positive individuals[20,24,25].

Building on previous evidence, a broad range of synaptic proteins has been examined in this study, spanning core SNARE complex proteins, 14-3-3 proteins, syntaxins (STX), NPTX, secretogranins (SCG), synucleins (Syn), synaptotagmins (Syt), vesicle trafficking proteins, as well as synaptic organization and adhesion proteins (Supplementary Table S1). Although associations between fluid synaptic proteins and abnormal amyloid biomarker profiles or global Aβ deposition have been investigated[15,16,26,27], limited data are available on synaptic protein relationships with regional Florbetapir PET amyloid burden. This study aimed (i) to identify SomaScan 7K–quantified CSF synaptic proteins associated with regional amyloid burden across predefined amyloid-relevant regions in mild cognitive impairment (MCI) individuals, and (ii) to examine whether these associations were independent of regional gray matter volume. CSF synaptic proteins would, as such, be informative as surrogate markers for spatiotemporal amyloid progression.

RESULTS

Participant characteristics

Participant demographic characteristics are summarized in Table 1. Of the 35 individuals with MCI, 80% were amyloid-PET positive, with most falling within the amyloid-positive range (SUVR ≥ 1.10; Supplementary Fig. S1). Regional SUVRs and gray matter volumes per VOI are reported in Supplementary Tables S4 and S5.

Table 1
Characteristics of the study population

Variable	MCI (n = 35)
Female, n (%)	13 (37.1%)
Age, years	69.25 ± 7.23
Education, years	15.20 ± 2.70
APOE ε4 carriers, n (%)	18 (51.4%)
Global amyloid, SUVR	1.35 ± 0.25
Amyloid positive, n (%)	28 (80.0%)

Continuous variables are presented as mean ± standard deviation (SD). Amyloid positivity was defined as a global standardized uptake value ratio (SUVR) ≥ 1.10. APOE, apolipoprotein E; MCI, mild cognitive impairment.

Associations of synaptic proteins with regional amyloid burden

As the primary analysis, elastic net regression, adjusted for age, sex, *APOE* ε4, and education, identified associations between synaptic proteins and amyloid burden across the n = 17 VOIs (Supplementary Table S6). Elastic net coefficients and mediation estimates for all protein–region associations are shown in Supplementary Fig. S2.

SNARE complex proteins

When exploring the core SNARE complex proteins, including SNAP-25, VAMP-2, and syntaxin-1A (STX-1A), associations for SNAP-25 and VAMP-2 were observed in limited cortical regions, with higher SNAP-25 associated with higher amyloid burden in the fusiform gyrus (β = 0.55, ADE = 0.38, $p_{FDR-corrected}$ = 0.005) and higher VAMP-2 levels associated with higher amyloid burden in the lateral temporal cortex-superior temporal gyrus (β = 1.45, ADE = 0.64, $p_{FDR-corrected}$ = 0.015) (Fig. 1a,b). Remarkably, STX-1A showed extensive positive associations with cerebral amyloid burden across multiple cortical regions, including the precuneus (β = 0.50, ADE = 0.48, $p_{FDR-corrected} = 5.62\times10^{-4}$), posterior cingulate gyrus (β = 0.42, ADE = 0.41, $p_{FDR-corrected}$ = 0.001), inferior parietal lobule–supramarginal gyrus (β = 0.43, ADE = 0.41, $p_{FDR-corrected}$ = 0.009), lateral temporal cortex–middle temporal gyrus (β = 0.47, ADE = 0.54, $p_{FDR-corrected}$ = 0.003), dorsolateral prefrontal cortex–superior frontal gyrus (β = 0.52, ADE = 0.52, $p_{FDR-corrected} = 3.24\times10^{-5}$), fusiform gyrus (β = 0.48, ADE = 0.85, $p_{FDR-corrected} = 6.79\times10^{-5}$), superior parietal lobule (β = 0.50, ADE = 0.45, $p_{FDR-corrected} = 4.59\times10^{-4}$), and cuneus (β = 0.42, ADE = 0.65, $p_{FDR-corrected} = 1.58\times10^{-6}$) (Fig. 1a,b).

14-3-3 proteins

Assessment of the 14-3-3 proteins showed associations with cerebral amyloid burden predominantly in the lateral temporal cortex–superior temporal gyrus (14-3-3 epsilon and eta: β = 4.28–12.47, ADE = 1.44–2.89; 14-3-3 beta/alpha: β=−14.76, ADE = − 3.55; $p_{\text{FDR–corrected}}$ = 0.015) and the fusiform gyrus (14-3-3 gamma, theta and sigma: β = 0.63–5.78, ADE = 0.77–3.08; 14-3-3 beta/alpha: β=−11.42, ADE = − 5.46; $p_{\text{FDR–corrected}}$ = 0.003) (Supplementary Fig. S3). 14-3-3 eta additionally showed an association in the putamen (β = 0.45, ADE = 0.42, $p_{\text{FDR–corrected}}$ = 0.002) (Supplementary Fig. S3).

Syntaxins

Within the Syntaxin group, STX-3 demonstrated associations in the inferior parietal lobule–angular gyrus (β = 0.39, ADE = 0.39, $p_{FDR–corrected}$ = 0.008), anterior cingulate gyrus (β = 0.41, ADE = 0.38, $p_{FDR–corrected}$ = 0.003) and lateral temporal cortex and superior temporal gyrus (β = 4.39, ADE = 1.33, $p_{FDR–corrected}$ = 0.003) (Fig. 2a,b). Whereas lower STX-7 associated with higher amyloid burden in the lateral temporal cortex–superior temporal gyrus (β=−4.89, ADE = − 1.24, $p_{FDR–corrected}$ = 0.033) (Fig. 2a,b).

Neuronal pentraxins and GluR4

Across the NPTX group, NPTXR and NPTX-1 associated with cerebral amyloid burden. Lower NPTXR associated with higher amyloid burden in the fusiform gyrus (β=−2.82, ADE = − 1.69, $p_{\text{FDR–corrected}}$ = 0.002), with an additional association in the caudate nucleus (β = 0.50, ADE = 0.49, $p_{\text{FDR–corrected}}$ = 0.003) (Fig. 2c,d). Lower NPTX-1 likewise associated with higher amyloid burden in the fusiform gyrus (β=−1.33, ADE = − 0.51, $p_{\text{FDR–corrected}}$ = 0.012) (Fig. 2c,d). In line with this, GluR4 positively associated with the lateral temporal cortex–superior temporal gyrus (β = 3.79, ADE = 1.35, $p_{\text{FDR–corrected}}$ = 0.003) and the fusiform gyrus (β = 1.18, ADE = 0.45, $p_{\text{FDR–corrected}}$ = 0.025) (Fig. 2c,d).

Secretogranins

In the SCG group, SCG-1 and SCG-3 associated with cerebral amyloid burden. Higher SCG-1 associated with higher amyloid burden in the fusiform gyrus (β = 1.30, ADE = 0.68, $p_{\text{FDR–corrected}} = 6.79\times10^{-5}$) (Supplementary Fig. S4). Higher SCG-3 associated with higher amyloid burden in the lateral temporal cortex–superior temporal gyrus (β = 1.93, ADE = 0.61, $p_{\text{FDR–corrected}}$ = 0.024) and the fusiform gyrus (β = 0.61, ADE = 0.60, $p_{\text{FDR–corrected}} = 6.31\times10^{-6}$) (Supplementary Fig. S4).

Synucleins

In the Syn group, lower Alpha-Syn and Gamma-Syn demonstrated association with higher cerebral amyloid burden. Specifically, Alpha-Syn associated with lateral temporal cortex–superior temporal gyrus

(β=−3.82, ADE = − 0.97, $p_{FDR-corrected}$ = 0.029) (Supplementary Fig. S4), whereas Gamma-Syn exhibited associations in the fusiform gyrus (β=−1.35, ADE = − 0.80, $p_{FDR-corrected}$ = 0.009) and cuneus (β=−0.59, ADE = − 0.52, $p_{FDR-corrected}$ = 2.46×10^{-4}) (Supplementary Fig. S4).

Synaptotagmins

Within the Syt group, Syt-2 and Syt-7 associated with cerebral amyloid burden. Higher Syt-2 associated with higher amyloid burden in the lateral temporal cortex–superior temporal gyrus (β = 1.77, ADE = 0.80, $p_{FDR-corrected}$ = 0.003) (Supplementary Fig. S5). On the other hand, lower Synaptotagmin-7 associated with higher amyloid burden in the dorsolateral prefrontal cortex–middle frontal gyrus (β=−0.18, ADE = − 0.19, $p_{FDR-corrected}$ = 2.57×10^{-12}) (Supplementary Fig. S5).

Synaptic vesicle pool regulation and trafficking proteins

Synaptogyrin-3 (Syngr-3), synaptic vesicle glycoprotein 2A (SV2A), and synapsin-3 (Syn-3) were identified as proteins significantly associated with cerebral amyloid burden, all of which play roles in vesicle pool regulation and trafficking. Higher Syngr-3 and SV2A associated with higher amyloid burden in the fusiform gyrus (Syngr-3: β = 1.32, ADE = 0.77, $p_{FDR-corrected}$ = 1.93×10^{-4}; SV2A: β = 0.62, ADE = 0.93, $p_{FDR-corrected}$ = 1.36×10^{-6}) (Supplementary Fig. S5). Syn-3 showed the most associations among these proteins, in the lateral temporal cortex–superior temporal gyrus (β = 0.88, ADE = 0.55, $p_{FDR-corrected}$ = 0.007), the dorsolateral prefrontal cortex–middle frontal gyrus (β=−0.31, ADE = − 0.21, $p_{FDR-corrected}$ = 1.62×10^{-15}) and the fusiform gyrus (β=−0.74, ADE = − 0.73, $p_{FDR-corrected}$ = 2.61×10^{-4}) (Supplementary Fig. S5).

Synaptic organization and adhesion proteins

Within the synaptic organization and adhesion proteins, calsyntenin-3 (Clstn-3), tenascin-R (TN-R), and Thy-1 membrane glycoprotein associated with cerebral amyloid burden. Among these, lower Clstn-3 associated with higher amyloid burden most broadly, in the posterior cingulate gyrus (β=−0.28, ADE = − 0.28, $p_{FDR-corrected}$ = 0.018), the fusiform gyrus (β=−0.36, ADE = − 0.59, $p_{FDR-corrected}$ = 1.36×10^{-6}), the superior parietal lobule (β=−0.42, ADE = − 0.33, $p_{FDR-corrected}$ = 0.003), and the caudate nucleus (β=−0.49, ADE = − 0.34, $p_{FDR-corrected}$ = 0.017) (Fig. 3a,b). Higher TN-R associated with lower amyloid burden in the lateral temporal cortex–superior temporal gyrus (β=−2.80, ADE = − 0.86, $p_{FDR-corrected}$ = 0.015) (Fig. 3a,b). Higher Thy-1 associated with higher amyloid burden in the lateral temporal cortex–superior temporal gyrus (β = 4.45, ADE = 1.34, $p_{FDR-corrected}$ = 0.003) and the fusiform gyrus (β = 2.31, ADE = 0.85, $p_{FDR-corrected}$ = 0.006) (Fig. 3a,b).

Mediation by gray matter volume

Mediation analyses were performed for all associations identified by elastic net regression, with regional gray matter volume as the mediator. None of the associations showed a significant indirect effect through gray matter volume, whereas all direct effects remained significant (all $p_{FDR-corrected} < 0.05$), indicating that the associations between CSF synaptic proteins and regional amyloid burden were independent of gray matter volume (Supplementary Fig. S2, Supplementary Table S7). The average direct effects are summarized per region in Fig. 4.

Summary of regional associations and protein intercorrelations

The associations between CSF synaptic proteins per region, ranging from early to late-stage amyloid-vulnerable VOIs, are summarized in Fig. 4. Overall, across synaptic proteins assessed, associations were most frequently observed in the fusiform gyrus as well as in the temporal cortex, accompanied by the highest effect sizes. STX-1A showed numerically the highest number of associations in VOIs spanning both early and later disease stages.

Additionally, intercorrelation analyses were performed to further investigate whether proteins associated with amyloid burden in specific regions were also intercorrelated. The partial Spearman coefficients between synaptic proteins are presented in Supplementary Tables S8 and S9, respectively. STX-1A and STX-3 showed the most intercorrelations, whereas Clstn-3, Syngr-3, and SCG-3 were not correlated with other synaptic proteins (Supplementary Tables S8 and S9).

DISCUSSION

Prior CSF studies have reported synaptic protein changes at the MCI or prodromal stage of AD, particularly in individuals who eventually develop dementia[28,29]. The current findings build on this, showing that these markers also track the regional distribution of amyloid pathology, which has so far been assessed with amyloid PET[4]. Among the analyzed synaptic proteins, CSF STX-1A and Clstn-3 were the most consistently associated with regional amyloid burden, showing associations from early through intermediate to later stages of amyloid deposition (summarized in Fig. 4)[5]. This consistency distinguishes STX-1A and Clstn-3 as promising candidates for tracking synaptic changes across the spatial progression of amyloid. Despite this shared sensitivity, these two proteins displayed distinct relationships with the broader CSF synaptic panel, suggesting they play complementary rather than overlapping roles. STX-1A was the most widely intercorrelated protein within the synaptic panel, which may relate to its central role in SNARE-mediated vesicle fusion[30]. Clstn-3, in contrast, was not associated with any other markers. As a synaptic adhesion protein involved in synapse formation and maintenance[31], it may represent a structural aspect of synaptic integrity. Together, they may provide a more complete view of synaptic dysfunction than either marker alone. In the posterior cingulate cortex, an early default-mode-network hub, and in the superior parietal lobule[32], higher CSF STX-1A and lower

CSF Clstn-3 were each linked with greater regional amyloid burden. The recurrence of this same pattern in regions affected both early and later in amyloid deposition argues against a local effect.

Beyond these two proteins, amyloid-synaptic associations were confined to certain proteins and specific regions (Fig. 4). Many proteins, across every functional group, were associated with amyloid burden in a single region, most often the superior temporal or fusiform gyrus. Conversely, several regions were associated with only one protein, such as STX-1A in the precuneus, supramarginal, middle temporal, and superior frontal gyri, and STX-3 in the angular gyrus and anterior cingulate cortex.

Regional differences in synaptic composition, protein expression, or vulnerability might explain why certain proteins are found to be associated in specific regions, a point that warrants further investigation. In two regions, the associations were much broader: The fusiform gyrus showed the largest number of associations, covering nearly every functional group examined, followed by the superior temporal gyrus. The fusiform gyrus is among the regions showing the highest amyloid deposition[33], suggesting that the large number of associations might reflect the extent of local amyloid involvement. In the dorsolateral prefrontal cortex, striatum, and occipital lobe, even adjacent subregions differed in the directionality of their effect regarding associated proteins (Fig. 4). For instance, higher CSF STX-1A was associated with greater amyloid burden in the superior frontal gyrus, whereas lower CSF Syt-7 and Syn-3 were associated with greater burden in the middle frontal gyrus, while occipital cortical associations were confined to the cuneus.

Several limitations should be considered when interpreting these findings. We made use of a mathematical tool, region-wise elastic net regression, to identify CSF proteins associated with amyloid load. The drawback is that the analysis was performed using mean regional amyloid SUVRs within each VOI rather than in a data-driven voxelwise manner without the need for a priori VOI selection. The latter would be computationally difficult, and this method is also not embedded in current versions of SPM. Moreover, parenchymal and vascular amyloid are not separable on amyloid-PET, and given that the occipital cortex is a predilection site for capillary cerebral amyloid angiopathy (CAA)[34], occipital associations may partly reflect CAA rather than parenchymal amyloid. The sample size was relatively small due to the strict time window between CSF collection and PET imaging, and only individuals at the MCI stage were included. This limits the ability to assess amyloid–synaptic protein associations across the entire AD continuum. Longitudinal, multi-stage cohorts will be needed to determine how these regional associations evolve from asymptomatic through dementia stages.

Overall, CSF synaptic proteins showed region-specific associations across early, intermediate, and late stages of amyloid deposition. STX-1A and Clstn-3 showed the most consistent associations across multiple stages of regional amyloid deposition. The heterogeneous protein profiles across brain regions indicate that synaptic protein–amyloid associations are not spatially uniform, highlighting the potential value of region-specific CSF synaptic markers. These findings support further evaluation of CSF synaptic proteins as potential surrogate markers of amyloid pathology when access to amyloid PET is limited.

METHODS

Participants

Data used in the preparation of this article were obtained from the Alzheimer's Disease Neuroimaging Initiative (ADNI) database (adni.loni.usc.edu). The ADNI was launched in 2003 as a public-private partnership, led by Principal Investigator Michael W. Weiner, MD. The primary goal of ADNI has been to test whether serial magnetic resonance imaging (MRI), positron emission tomography (PET), other biological markers, and clinical and neuropsychological assessment can be combined to measure the progression of mild cognitive impairment (MCI) and early Alzheimer's disease (AD). For up-to-date information, see www.adni-info.org.

The ADNI study protocols were approved by the institutional review boards of all participating institutions, and written informed consent was obtained from all participants or their legally authorized representatives in accordance with the Declaration of Helsinki. The present study was a secondary analysis of de-identified ADNI data and involved no new participant recruitment or data collection. All methods were carried out in accordance with relevant guidelines and regulations.

The study population included 35 MCI individuals from the Alzheimer's Disease Neuroimaging Initiative (ADNI)[35] (Supplementary Table S2). Individuals were initially selected from a cohort whose CSF samples had been analyzed using the SomaScan platform, similar to the dataset reported by Guo et al.[36] 'Guo_2024_41562_2024_1924_MOESM5_ESM.CSV'[37]. Among these individuals, those with available baseline [^{18}F] Florbetapir (AV-45) amyloid PET scans were included, after which the MRI scan closest to the baseline PET acquisition was identified. Individuals were included such that the time intervals between baseline MRI and baseline PET acquisition, between baseline PET acquisition and CSF measurement, and between MRI acquisition and CSF measurement were no longer than approximately 5, 8, and 11 months, respectively.

Imaging acquisition and analysis

PET processing

Cerebral amyloid deposition was assessed using [^{18}F] Florbetapir (AV-45) PET, acquired between 50–70 min post-injection on ADNI-qualified PET/CT scanners according to ADNI protocols.[38] Acquisition and reconstruction details are provided in the Supplementary Methods.

After conversion to NIfTI format (Supplementary Methods), MRI/PET scans were processed using SPM12 (Wellcome Centre for Human Neuroimaging, London, UK), executed under MATLAB version R2022b (MathWorks, Natick, MA, USA). Amyloid PET quantification was performed using an in-house automated pipeline applied across all subjects organized in a BIDS-like directory structure. The MRI and

PET scans for each subject were reoriented by adjusting the image origin to the anterior commissure–posterior commissure (AC–PC) line to achieve alignment in Montreal Neurological Institute (MNI) space. PET frames were realigned to their mean image. Frames exhibiting translational displacement greater than 6 mm or rotational displacement greater than 6° were excluded from subsequent analyses. Three participants were excluded for excessive head motion during PET acquisition.

The mean PET image was calculated and co-registered to the T1-weighted MRI image. MRI scans underwent tissue segmentation, and spatial normalization parameters derived from the MRI processing were then applied to normalize the PET frames to MNI space. Volumes of interest (VOIs) were defined using the Brainnetome atlas[39] and selected based on previously well-established amyloid progression patterns, including cortical and striatal amyloid PET staging approaches[5,9,33,40,41] and regions vulnerable to early amyloid deposition in default mode network nodes[6–8]. A total of n = 17 VOIs covered medial parietal, cingulate, frontal, lateral temporal, parietal, fusiform, occipital, and striatal regions (Supplementary Table S3). Mean standardized uptake value ratios (SUVRs) within VOIs were calculated over the 50–70 min post-injection interval, with the whole cerebellum used as the reference region. The distribution of amyloid burden within our cohort was examined with histograms and using a positivity cut-off of SUVR ≥ 1.10[42].

MRI processing

T1-weighted MRI scans were acquired at 3T (Siemens and Philips) using the standardized ADNI 3D MPRAGE protocol (flip angle 9°; isotropic voxels of approximately 1–1.2 mm), using the scan closest to PET for each participant. Absolute gray matter (GM) and total intracranial volume (TIV) were estimated through tissue segmentation with the Computational Anatomy Toolbox (CAT12) in SPM12. Modulated GM volumes for each individual were divided by TIV to account for inter-individual variation in intracranial volume. To assess atrophy in the set of n = 17 VOIs, GM volumes within each VOI were calculated from modulated GM maps using an intensity threshold greater than 0.3 [43]. These GM volumes were used in further mediation analyses to assess the direct and indirect effects of CSF synaptic proteins on amyloid deposition.

CSF measurements

Detailed information on CSF handling and analysis has been described previously[36,44,45]. Roche Elecsys and cobas e 601 automated immunoassay analyzer systems were used for measuring the levels of $A\beta_{42}$ in CSF[44,45].

For synaptic proteins, CSF proteomic data were previously obtained using the SOMAmer-based capture array assay (SomaScan 7K platform),[37] a high-throughput proteomic technology that allows parallel measurement of thousands of human proteins across a wide femtomolar-to-micromolar dynamic

range[46]. The protein levels in CSF were reported as relative fluorescence units (RFU). Data normalization was performed by SomaLogic. Based on empirical evidence,[23,25,47,48] 35 synaptic proteins identified as AD-associated markers were selected. Of these, synaptic proteins differentially expressed between biologically defined AD (amyloid-β and p-tau181 positive, A + T+) and cognitively normal A–T– individuals in a previous study [36] were retained. The retained synaptic proteins were then extracted from the SomaScan 7K proteomic dataset (Supplementary Table S1).

Statistical analysis

All statistical analyses were performed in R (version 4.5.0) or Python (version 3.13.2). As a primary analysis, region-wise elastic net regression (R package 'glmnet') was applied to identify CSF proteins associated with mean regional amyloid SUVRs within each VOI (Supplementary Table S3). Results were stratified based on each protein's biological category, i.e., SNARE complex, 14-3-3 proteins, STX, NPTX, SCG, Syn, Syt, vesicle trafficking proteins, as well as synaptic organization and adhesion, respectively. Unlike ordinary linear regression, elastic net performs automatic variable selection, retaining only a subset of proteins in the fitted model. The mixing parameter α, which balances lasso (α = 1) and ridge (α → 0) penalization, and the regularization strength λ, which controls the overall amount of coefficient shrinkage, were evaluated over predefined grids (α = 1, 0.8, 0.6, 0.4, 0.2, 0.1; λ = 1 to 0.001 in steps of 0.001, and 0.0001).

Post-selection statistical inference was performed in R ('stats' package) simultaneously for all associations selected by elastic net using linear regression adjusted for age, sex, *APOE* ε4, and education to obtain coefficient estimates, confidence intervals, and p-values that account for variable selection. Statistical significance was evaluated after correction for the number of VOIs using the Benjamini–Hochberg false discovery rate (FDR) procedure.

As a secondary analysis, mediation analyses adjusted for age, sex, *APOE* ε4, and education were performed concurrently across all significant associations identified by elastic net regression to assess whether these were influenced by regional atrophy, as indexed by GM volume in each VOI. All associations were evaluated using unidirectional mediation analysis with gray matter volume as the mediator within a unified structural equation modelling framework implemented in R ('lavaan' package). Particular emphasis was placed on estimating the biological direct effects, and CSF proteins showing statistically significant average direct effects (ADE) were interpreted as associations independent of gray matter loss. All mediation results were corrected for multiple comparisons using FDR adjustments.

For the proteins demonstrating significant associations with amyloid burden independent of gray matter volume, intercorrelation analyses using partial Spearman correlations adjusted for age, sex, *APOE* ε4, and education were additionally performed. This analysis was conducted to further investigate whether proteins associated with amyloid burden in specific regions were also intercorrelated. Details of data visualization methods are described in the Supplementary Methods.

Declarations

COMPETING INTERESTS

The authors declare no competing interests.

FUNDING

Data collection and sharing for the Alzheimer's Disease Neuroimaging Initiative (ADNI) is funded by the National Institute on Aging (National Institutes of Health Grant U19 AG024904). The grantee organization is the Northern California Institute for Research and Education. In the past, ADNI has also received funding from the National Institute of Biomedical Imaging and Bioengineering, the Canadian Institutes of Health Research, and private sector contributions through the Foundation for the National Institutes of Health (FNIH) including generous contributions from the following: AbbVie, Alzheimer's Association; Alzheimer's Drug Discovery Foundation; Araclon Biotech; BioClinica, Inc.; Biogen; Bristol-Myers Squibb Company; CereSpir, Inc.; Cogstate; Eisai Inc.; Elan Pharmaceuticals, Inc.; Eli Lilly and Company; EuroImmun; F. Hoffmann-La Roche Ltd and its affiliated company Genentech, Inc.; Fujirebio; GE Healthcare; IXICO Ltd.; Janssen Alzheimer Immunotherapy Research & Development, LLC.; Johnson & Johnson Pharmaceutical Research & Development LLC.; Lumosity; Lundbeck; Merck & Co., Inc.; Meso Scale Diagnostics, LLC.; NeuroRx Research; Neurotrack Technologies; Novartis Pharmaceuticals Corporation; Pfizer Inc.; Piramal Imaging; Servier; Takeda Pharmaceutical Company; and Transition Therapeutics. Generation and quality control of the CSF SomaScan 7K data were supported by the National Institutes of Health [grant numbers RF1 AG074007, R01 AG044546, P01 AG003991, RF1 AG053303, RF1 AG058501, U01 AG058922]; the Chan Zuckerberg Initiative; and the Alzheimer's Association [Zenith Fellows Award ZEN-22-848604]. JS received personal funding from the Fonds Wetenschappelijk Onderzoek (FWO/Belgium) [senior postdoctoral fellowship to JS, grant number 12Y1623N]. The funding organizations had no role in study design; in the collection, analysis, and interpretation of data; in the writing of the report; or in the decision to submit the article for publication.

Author Contribution

All authors contributed to the conception and design of the study. S.A. and J.S. retrieved and selected the SomaScan and Florbetapir PET data from ADNI. S.A., P.B., and P.A. performed the data and statistical analyses. All authors interpreted the results. S.A., P.B., and J.S. drafted the manuscript. J.S. and K.P. supervised the study and provided critical revision of the manuscript for important intellectual content. All authors revised the text, tables, and figures and approved the final version.

Acknowledgement

Data used in preparation of this article were obtained from the Alzheimer's Disease Neuroimaging Initiative (ADNI) database (adni.loni.usc.edu). As such, the investigators within the ADNI contributed to the design and implementation of ADNI and/or provided data but did not participate in analysis or writing of this report. A complete listing of ADNI investigators can be found at: http://adni.loni.usc.edu/wp-content/uploads/how_to_apply/ADNI_Acknowledgement_List.pdfThe CSF SomaScan 7K proteomic data used in this study were generated by the NeuroGenomics and Informatics Center and the Cruchaga Lab at Washington University School of Medicine. We thank Prof. dr. Patrick Dupont for the development of SPM image processing scripts in Matlab.

Data Availability

The data used in this study are available from the Alzheimer's Disease Neuroimaging Initiative (ADNI) database (adni.loni.usc.edu), subject to registration and approval through ADNI's Data Sharing and Publication Committee under the ADNI Data Use Agreement. The analysis scripts used in this study are available from the corresponding author upon reasonable request.

References

1. Hampel, H. et al. The Amyloid-β Pathway in Alzheimer’s Disease. *Mol. Psychiatry*. **26**, 5481–5503 (2021).
2. Rowe, C. C. & Villemagne, V. L. Brain Amyloid Imaging. *J. Nucl. Med.* **52**, 1733–1740 (2011).
3. Pemberton, H. G. et al. Quantification of amyloid PET for future clinical use: a state-of-the-art review. *Eur. J. Nucl. Med. Mol. Imaging*. **49**, 3508–3528 (2022).
4. Leuzy, A. et al. Considerations in the clinical use of amyloid PET and CSF biomarkers for Alzheimer’s disease. *Alzheimers Dement.* **21**, e14528 (2025).
5. Grothe, M. J. et al. In vivo staging of regional amyloid deposition. *Neurology* **89**, 2031–2038 (2017).
6. Ingala, S. et al. Amyloid-driven disruption of default mode network connectivity in cognitively healthy individuals. *Brain Commun.* **3**, fcab201 (2021).
7. Sperling, R. A. et al. Amyloid Deposition Is Associated with Impaired Default Network Function in Older Persons without Dementia. *Neuron* **63**, 178–188 (2009).
8. Palmqvist, S. et al. Earliest accumulation of β-amyloid occurs within the default-mode network and concurrently affects brain connectivity. *Nat. Commun.* **8**, 1214 (2017).
9. Hanseeuw, B. J. et al. PET staging of amyloidosis using striatum. *Alzheimers Dement.* **14**, 1281–1292 (2018).
10. Palop, J. J. & Mucke, L. Amyloid-β–induced neuronal dysfunction in Alzheimer’s disease: from synapses toward neural networks. *Nat. Neurosci.* **13**, 812–818 (2010).
11. Taddei, R. N. & Duff, E. Synapse vulnerability and resilience underlying Alzheimer’s disease. *EBioMedicine* **112**, 105557 (2025).

12. McGeachan, R. I. et al. Divergent actions of physiological and pathological amyloid-β on synapses in live human brain slice cultures. *Nat. Commun.* **16**, 3753 (2025).
13. Melgosa-Ecenarro, L. et al. Selective weakening of population-coupled synaptic activity in vivo in a mouse model of amyloid-beta pathology. *Nat. Commun.* **17**, 3646 (2026).
14. Cai, W., Li, L., Sang, S., Pan, X. & Zhong, C. Physiological Roles of β-amyloid in Regulating Synaptic Function: Implications for AD Pathophysiology. *Neurosci. Bull.* **39**, 1289–1308 (2023).
15. Goossens, J. et al. Evaluation of cerebrospinal fluid levels of synaptic vesicle protein, VAMP-2, across the sporadic Alzheimer's disease continuum. *Alzheimers Res. Ther.* **15**, 186 (2023).
16. Das, S. et al. Synaptic biomarkers in the cerebrospinal fluid associate differentially with classical neuronal biomarkers in patients with Alzheimer's disease and frontotemporal dementia. *Alzheimers Res. Ther.* **15**, 62 (2023).
17. Belbin, O. et al. Cerebrospinal fluid profile of NPTX2 supports role of Alzheimer's disease-related inhibitory circuit dysfunction in adults with Down syndrome. *Mol. Neurodegener*. **15**, 46 (2020).
18. Brinkmalm, A. et al. SNAP-25 is a promising novel cerebrospinal fluid biomarker for synapse degeneration in Alzheimer's disease. *Mol. Neurodegener*. **9**, 53 (2014).
19. Lleó, A. et al. Changes in Synaptic Proteins Precede Neurodegeneration Markers in Preclinical Alzheimer's Disease Cerebrospinal Fluid. *Mol. Cell. Proteom.* **18**, 546–560 (2019).
20. Nilsson, J. et al. Cerebrospinal fluid biomarker panel of synaptic dysfunction in Alzheimer's disease and other neurodegenerative disorders. *Alzheimers Dement.* **19**, 1775–1784 (2023).
21. Oeckl, P. et al. Blood β-synuclein is related to amyloid PET positivity in memory clinic patients. *Alzheimers Dement.* **19**, 4896–4907 (2023).
22. Lu, Y. Early increase of cerebrospinal fluid 14-3-3ζ protein in the alzheimer's disease continuum. *Front. Aging Neurosci.* **14**, 941927 (2022).
23. Qiang, Q. et al. CSF 14-3-3β is associated with progressive cognitive decline in Alzheimer's disease. *Brain Commun.* **5**, fcad312 (2023).
24. Xiao, M. F. et al. NPTX2 and cognitive dysfunction in Alzheimer's Disease. *eLife*6, e23798 (2017).
25. Soldan, A. et al. NPTX2 in Cerebrospinal Fluid Predicts the Progression From Normal Cognition to Mild Cognitive Impairment. *Ann. Neurol.* **94**, 620–631 (2023).
26. Milà-Alomà, M. et al. CSF Synaptic Biomarkers in the Preclinical Stage of Alzheimer Disease and Their Association With MRI and PET. *Neurology* **97**, e2065–e2078 (2021).
27. Palmqvist, S. et al. Cerebrospinal fluid and plasma biomarker trajectories with increasing amyloid deposition in Alzheimer's disease. *EMBO Mol. Med.* **11**, e11170 (2019).
28. Duits, F. H. et al. Synaptic proteins in CSF as potential novel biomarkers for prognosis in prodromal Alzheimer's disease. *Alzheimers Res. Ther.* **10**, 5 (2018).
29. Portelius, E. et al. Cerebrospinal fluid neurogranin: relation to cognition and neurodegeneration in Alzheimer's disease. *Brain* **138**, 3373–3385 (2015).

30. Südhof, T. C. Neurotransmitter Release: The Last Millisecond in the Life of a Synaptic Vesicle. *Neuron* **80**, 675–690 (2013).
31. Pettem, K. L. et al. The Specific α-Neurexin Interactor Calsyntenin-3 Promotes Excitatory and Inhibitory Synapse Development. *Neuron* **80**, 113–128 (2013).
32. Kim, H. H. et al. Exploration of neuroanatomical characteristics to differentiate prodromal Alzheimer's disease from cognitively unimpaired amyloid-positive individuals. *Sci. Rep.* **14**, 10083 (2024).
33. Lecy, E. E. et al. Patterns of Early Neocortical Amyloid-β Accumulation: A PET Population-Based Study. *J. Nucl. Med.* **65**, 1122–1128 (2024).
34. Gawor, K., Statz, K., Schaeverbeke, J. & Thal, D. R. Alzheimer's disease subtyping approaches and the role of co-pathologies. *Brain J. Neurol.* **149**, 2936–2954 (2026).
35. Petersen, R. C. et al. Alzheimer's Disease Neuroimaging Initiative (ADNI). *Neurology* **74**, 201–209 (2010).
36. Guo, Y. et al. Multiplex cerebrospinal fluid proteomics identifies biomarkers for diagnosis and prediction of Alzheimer's disease. *Nat. Hum. Behav.* **8**, 2047–2066 (2024).
37. Yang, C. et al. Genomic atlas of the proteome from brain, CSF and plasma prioritizes proteins implicated in neurological disorders. *Nat. Neurosci.* **24**, 1302–1312 (2021).
38. Jagust, W. J. et al. The Alzheimer's Disease Neuroimaging Initiative 2 PET Core: 2015. *Alzheimers Dement.* **11**, 757–771 (2015).
39. Fan, L. et al. The Human Brainnetome Atlas: A New Brain Atlas Based on Connectional Architecture. *Cereb. Cortex*. **26**, 3508–3526 (2016).
40. Pascoal, T. A. et al. Topographical distribution of Aβ predicts progression to dementia in Aβ positive mild cognitive impairment. *Alzheimers Dement. Diagn. Assess. Dis. Monit.* **12**, e12037 (2020).
41. Mattsson, N. et al. Independent information from cerebrospinal fluid amyloid-β and florbetapir imaging in Alzheimer's disease. *Brain* **138**, 772–783 (2015).
42. Joshi, A. D. et al. Performance characteristics of amyloid PET with florbetapir F 18 in patients with alzheimer's disease and cognitively normal subjects. *J. Nucl. Med.* **53**, 378–384 (2012).
43. Schaeverbeke, J. M. et al. Baseline cognition is the best predictor of 4-year cognitive change in cognitively intact older adults. *Alzheimers Res. Ther.* **13**, 75 (2021).
44. Bittner, T. et al. Technical performance of a novel, fully automated electrochemiluminescence immunoassay for the quantitation of β-amyloid (1–42) in human cerebrospinal fluid. *Alzheimers Dement.* **12**, 517–526 (2016).
45. Irwin, D. J. et al. Evolution of Alzheimer's Disease Cerebrospinal Fluid Biomarkers in Early Parkinson's Disease. *Ann. Neurol.* **88**, 574–587 (2020).
46. Candia, J., Daya, G. N., Tanaka, T., Ferrucci, L. & Walker, K. A. Assessment of variability in the plasma 7k SomaScan proteomics assay. *Sci. Rep.* **12**, 17147 (2022).

47. Lleó, A. et al. VAMP-2 is a surrogate cerebrospinal fluid marker of Alzheimer-related cognitive impairment in adults with Down syndrome. *Alzheimers Res. Ther.* **13**, 119 (2021).

48. Nilsson, J. et al. Cerebrospinal fluid biomarker panel for synaptic dysfunction in a broad spectrum of neurodegenerative diseases. *Brain* **147**, 2414–2427 (2024).

Figures

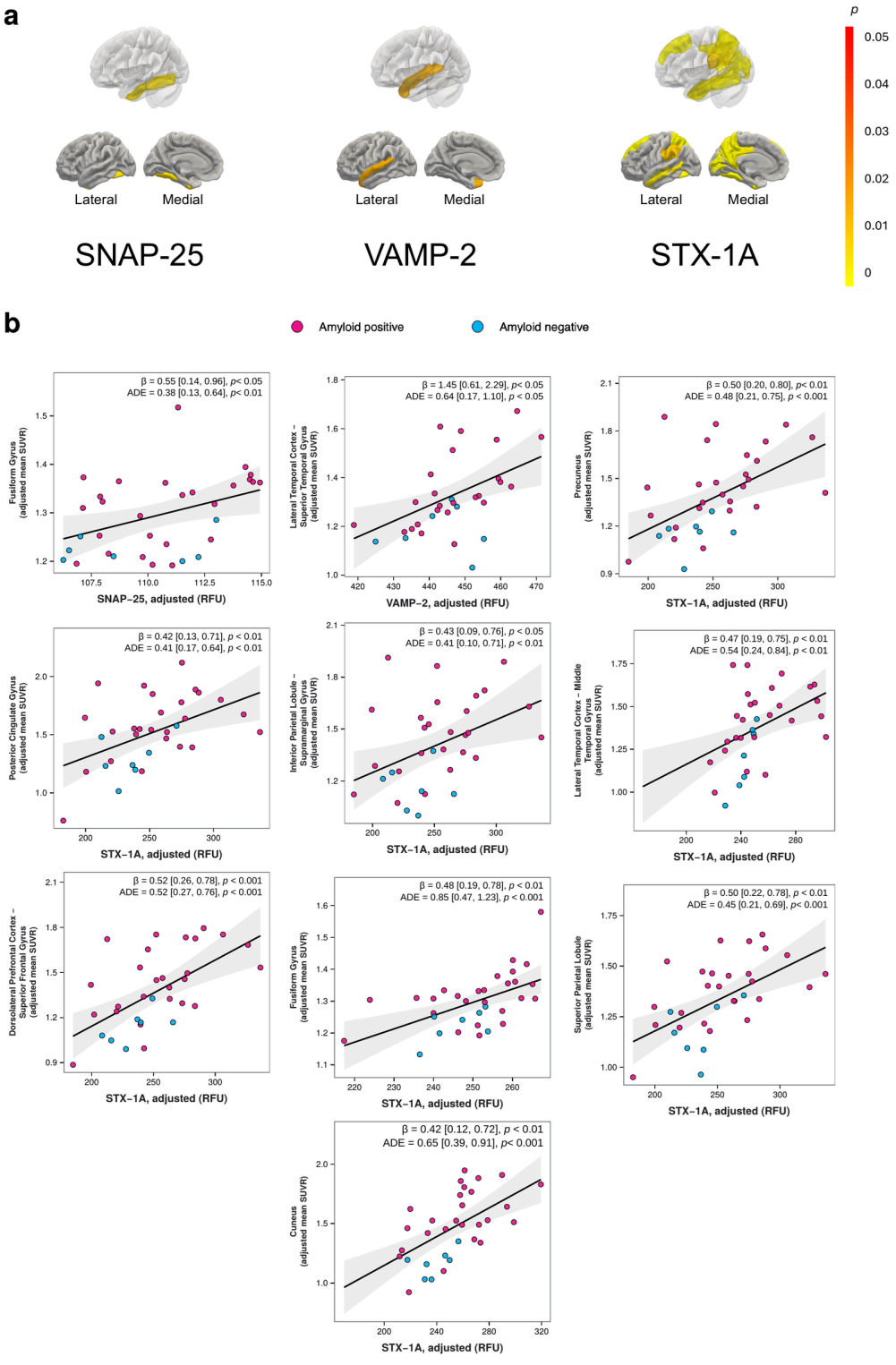

Figure 1

Regional amyloid associations with core soluble N-ethylmaleimide-sensitive factor attachment protein receptor (SNARE) proteins: synaptosomal-associated protein 25 (SNAP-25), vesicle-associated membrane protein 2 (VAMP-2), and syntaxin-1A (STX-1A). **a**Regional associations for each protein, shown on the left hemisphere as a 3D rendering (top) and on the lateral and medial cortical surfaces (bottom); regional values are bilateral means. The color bar indicates Benjamini-Hochberg false discovery rate (FDR)-corrected p-values. **b** Scatter plots showing the associations of cerebrospinal fluid (CSF) SNAP-25, VAMP-2, and STX-1A levels with regional amyloid burden. CSF protein levels (relative fluorescence units, RFU) and regional amyloid burden (mean standardized uptake value ratio, SUVR) are shown adjusted for age, sex, APOE ε4, education, and the other proteins selected in the same region (added-variable plots); the regression line therefore reflects the adjusted association. The gray shaded area represents the 95% confidence interval around the regression line. Blue dots: amyloid-negative; red dots: amyloid-positive cases.

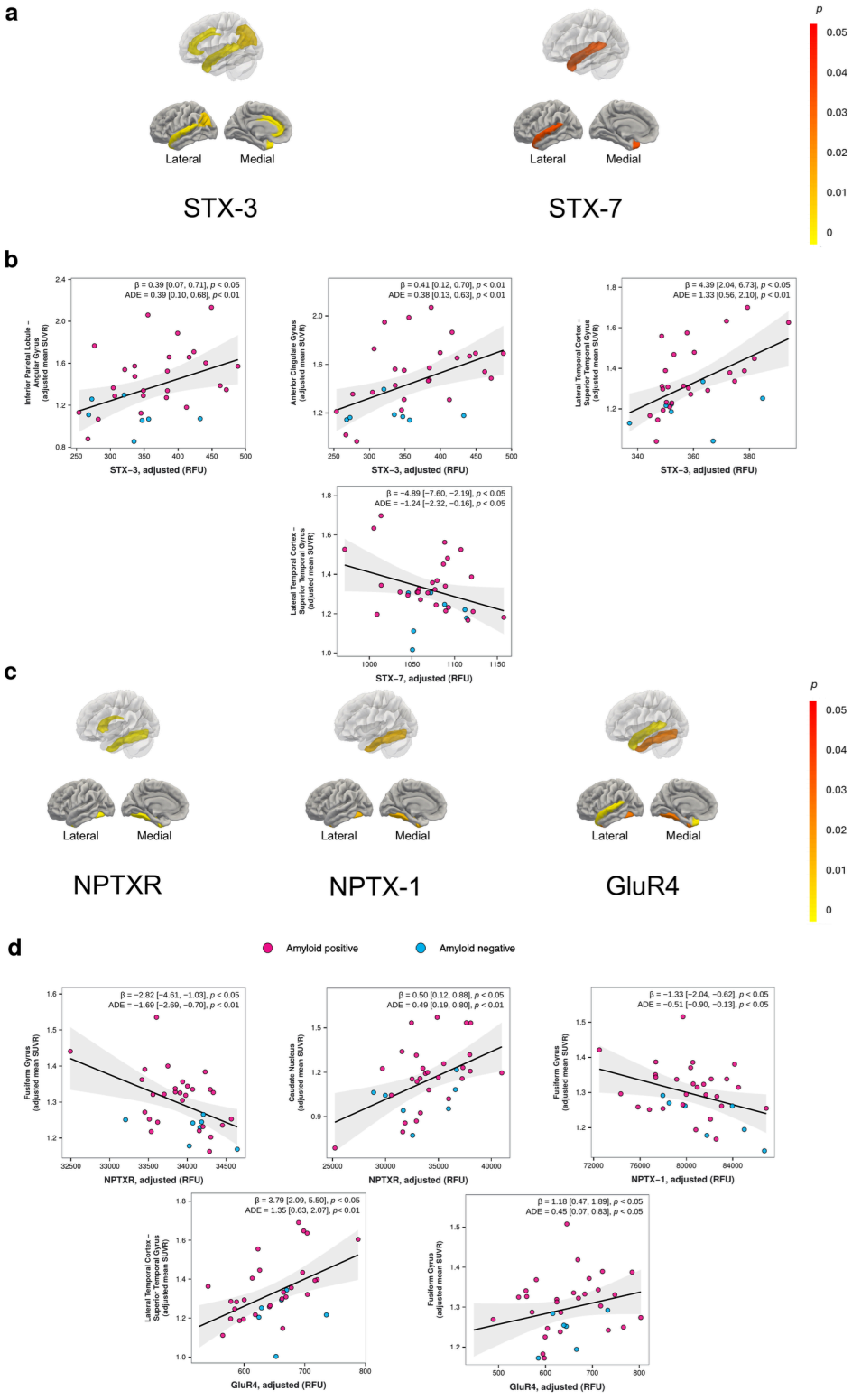

Figure 2

Regional amyloid associations with syntaxin-3 (STX-3), syntaxin-7 (STX-7), neuronal pentraxin receptor (NPTXR), neuronal pentraxin-1 (NPTX-1), and glutamate receptor 4 (GluR4). **a**Regional associations for STX-3 and STX-7, shown on the left hemisphere as a 3D rendering (top) and on the lateral and medial cortical surfaces (bottom); regional values are bilateral means. The color bars indicate Benjamini–Hochberg false discovery rate (FDR)-corrected p-values. **b** Scatter plots showing the associations of

cerebrospinal fluid (CSF) STX-3 and STX-7 levels with regional amyloid burden. **c** Regional associations for NPTXR, NPTX-1, and GluR4, shown as in **a**. **d**Scatter plots showing the associations of CSF NPTXR, NPTX-1, and GluR4 levels with regional amyloid burden. CSF protein levels (relative fluorescence units, RFU) and regional amyloid burden (mean standardized uptake value ratio, SUVR) are shown adjusted for age, sex, APOE ε4, education, and the other proteins selected in the same region (added-variable plots); the regression lines therefore reflect the adjusted associations. The gray shaded areas represent the 95% confidence intervals around the regression lines. Blue dots: amyloid-negative; red dots: amyloid-positive cases.

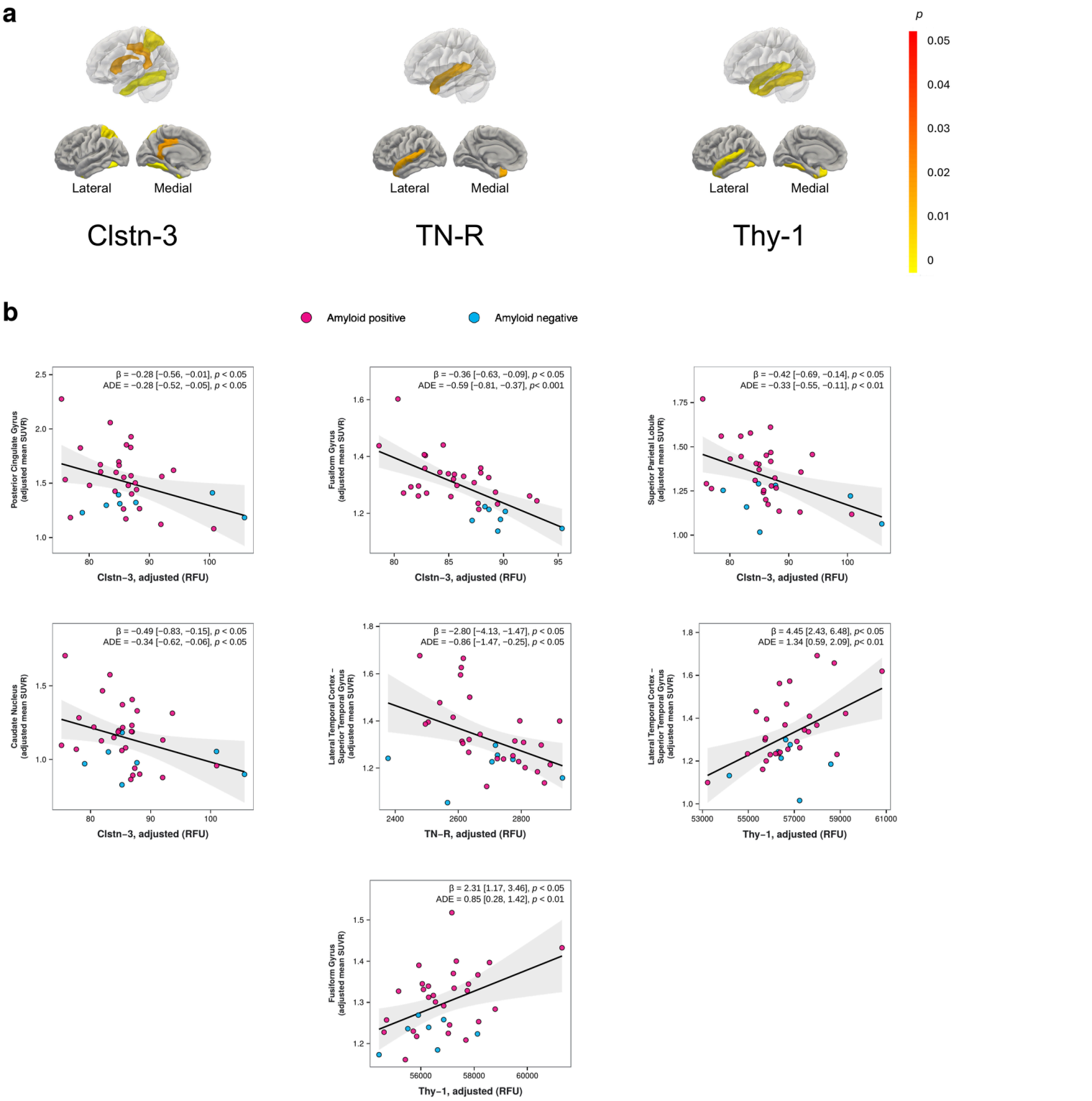

Figure 3

Regional amyloid associations with the synaptic organization and adhesion proteins: calsyntenin-3 (Clstn-3), tenascin-R (TN-R), and Thy-1 membrane glycoprotein (Thy-1). **a** Regional associations for each protein, shown on the left hemisphere as a 3D rendering (top) and on the lateral and medial cortical surfaces (bottom); regional values are bilateral means. The color bar indicates Benjamini-Hochberg false discovery rate (FDR)-corrected p-values. **b** Scatter plots showing the associations of cerebrospinal fluid

(CSF) Clstn-3, TN-R, and Thy-1 levels with regional amyloid burden. CSF protein levels (relative fluorescence units, RFU) and regional amyloid burden (mean standardized uptake value ratio, SUVR) are shown adjusted for age, sex, APOE ε4, education, and the other proteins selected in the same region (added-variable plots); the regression line therefore reflects the adjusted association. The gray shaded area represents the 95% confidence interval around the regression line. Blue dots: amyloid-negative; red dots: amyloid-positive cases.

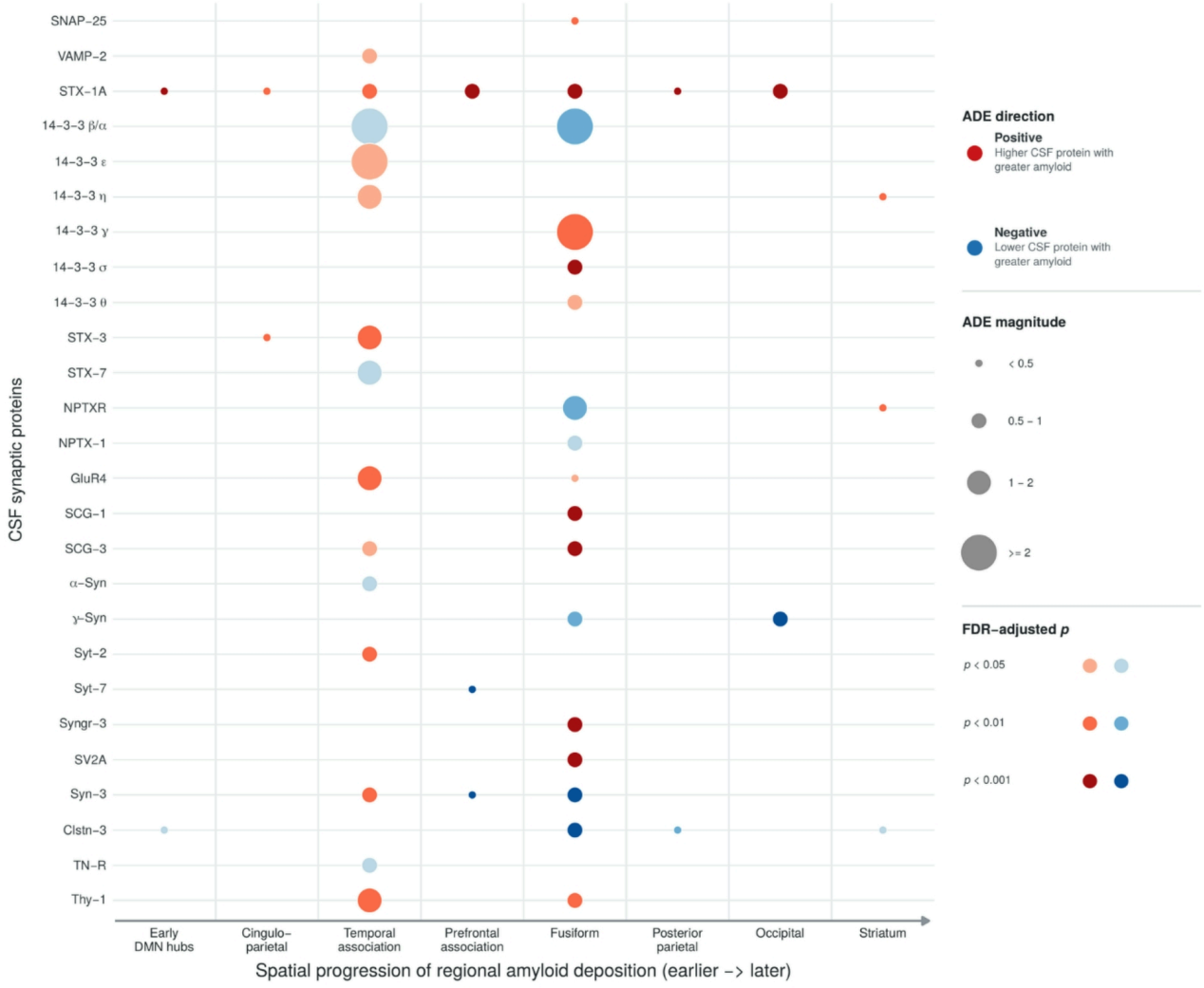

Figure 4

Spatial distribution of associations between CSF synaptic proteins and regional amyloid burden. Significant protein-region associations independent of gray matter volume were identified through mediation analysis and are shown according to their average direct effects (ADEs). Red indicates a positive ADE, with higher CSF protein levels associated with greater amyloid burden, whereas blue indicates a negative ADE, with lower CSF protein levels associated with greater amyloid burden. Darker

shades represent lower FDR-corrected p-values, while point size represents the absolute magnitude of the ADE.

Supplementary Files

This is a list of supplementary files associated with this preprint. Click to download.

- Table1ADNIsynapticproteinsAlalietalSCreports26.docx
- SupAlalietalSCreports26final.pdf